Proceedings of the ASME Turbo Expo 2017: Turbine Technical Conference and Exposition
GT2017
June 26-30, 2017, Charlotte, NC, USA

GT2017-63441

EXPERIMENTAL SENSITIVITY ANALYSIS AND THE EQUIVALENCE OF PULSED FORCING AND FEEDBACK CONTROL IN THERMOACOUSTIC SYSTEMS

Nicholas P. Jamieson*

Department of Engineering
University of Cambridge
Cambridge, United Kingdom CB21PZ
Email: npj24@cam.ac.uk

Matthew P. Juniper

Department of Engineering
University of Cambridge
Cambridge, United Kingdom CB21PZ
Email: mpj1001@cam.ac.uk

ABSTRACT

We examine the shifts in linear decay rates and growth rates, with and without control devices on a simple thermoacoustic system. When the system is stable, we measure the decay rate by pulsing with a loudspeaker. This improves on the experimental techniques developed by Rigas et al. (J. Fluid Mech., 2016, vol. 787, R1 [1]) and Jamieson et al. (Int. J. Spray and Comb. Dyn., accepted, 2016 [2]), to develop a more efficient method of experimental sensitivity analysis to apply in thermoacoustic systems. When the system is unstable, we use feedback control to bring it to a non-oscillating state. We then switch off the feedback control and measure the growth rate. The results suggest that both methods are suitable for use in the experimental sensitivity analysis of thermoacoustic systems. Our experimental set up is automated and we find that we can obtain thousands of decay rates in 1/12 the time compared with the previous work.

NOMENCLATURE

$A(t)$ Instantaneous amplitude of Hilbert transform.
D_i Iris diameter.
D_t Rijke tube diameter.
FBC Feedback control.
L Length of the Rijke tube.
PFM Pulsed forcing method.
PSD Power spectral density.
P_1 Primary heater power.
$P_{1,Hopf}$ Primary heater power at which system becomes linearly unstable.
P_2 Secondary heater power.
p' Pressure fluctuation.
$\dot{q}'$ Heat release rate fluctuation.
v' Velocity fluctuation.
x_c/L Normalised position of control device.
x_p/L Normalised position of the primary heater.
$\phi(t)$ Instantaneous phase of Hilbert transform.
σ_r Growth rate if positive, decay rate if negative.
$\sigma_{r,0}$ Baseline growth or decay rate.
$\sigma_{r,c}$ Controlled growth or decay rate.
$\delta\sigma_r$ Shift in growth or decay rate.

1 INTRODUCTION

Thermoacoustic oscillations occur in many combustion systems. The oscillations are often characterized by high amplitude pressure oscillations whose frequency is close to that of the resonant acoustic modes of the combustion system. Thermoacoustic oscillations arise due to feedback between acoustic waves and unsteady heat release rate when the heat release rate is in phase with the unsteady pressure. Thermoacoustic oscillations can be dangerous and threaten the performance and reliability of combustion systems by increasing the risks of mechanical vibration, thrust oscillations, or even complete failure [3]. The mitigation

*Address all correspondence to this author.

of thermoacoustic oscillations has become an important consideration for gas turbine manufacturers. Legislation to reduce the level of NO_x emission is leading manufacturers to adopt lean premixed combustion, but this also causes combustors to be more susceptible to thermoacoustic oscillations [4].

There are two main aims of this paper. Firstly, we investigate passive control of an electrically heated Rijke tube via (i) a passive drag device, and (ii) a secondary heater. The main novelty is that we extend the work of [1] and [2] to develop a more efficient method for experimental sensitivity analysis in thermoacoustics. Secondly, we show that results from the pulsed forcing method and the feedback control method extrapolate to nearly the same regions of zero growth rate, highlighting both methods' suitability for use in the experimental sensitivity analysis of thermoacoustic systems.

1.1 Rijke tube and control

The Rijke tube, first proposed by [5], is a laboratory-scale experiment through which the physics of thermoacoustic systems can be studied [6]. To explain the mechanism, it is convenient to consider the first acoustic mode, assuming that the pressure perturbation is zero at both ends, and neglecting the mean heat release rate from the heater. This mode has a pressure node and velocity antinode at each end of the tube, and a pressure antinode and velocity node in the middle. During the compression phase of the acoustic cycle, the acoustic velocity is towards the middle. When the Rijke tube is vertical, natural convection causes a mean upwards velocity. When the heater is in the bottom half of the tube, the acoustic velocity and mean velocity are therefore in the same direction during the compression phase. This causes an increased heat transfer rate from the wire to the flow. There is also a small time delay [7] between the velocity and the subsequent heat transfer rate. Put together, this causes there to be a slightly higher heat release rate during moments of higher pressure than there is during moments of lower pressure. This causes more mechanical work to be done by the gas expanding during the expansion phase than was required to compress it during the compression phase [8]. The amplitude of acoustic oscillations grow until the excess work is dissipated through acoustic radiation and viscous/thermal losses, characterised by a stable limit-cycle.

There are two types of control which are typically used to mitigate thermoacoustic oscillations: passive control and active feedback control [9–11]. Passive control can be implemented by changing the design of a system, or incorporating additional devices, such as Helmholtz resonators and baffles. For example, thermoacoustic oscillations in the F1 engine of the Saturn V rocket were suppressed by adding baffles to the injector plate [12]. An extension of passive control is tuned passive control, in which the characteristics of the passive device can be altered after installation, for example by changing the volume or throat area of a Helmholtz resonator. Two of the devices described in this paper, an iris and a secondary heater, are best described as tuned passive control. Tuned passive control via a secondary heater is described by [13] and [14]. These studies showed that a secondary heater placed at certain positions downstream of a flame in a duct could suppress thermoacoustic oscillations. In the work of [13], it was found that a secondary heater located at $x/L = 0.75$ had a stabilising effect on the system when the primary heater was located at $x/L = 0.25$. Regarding feedback control, one of the earliest applications to thermoacoustics was by [15]. In this study a system consisting of a microphone upstream of the heater, which records a signal that is then phase-shifted, amplified and transmitted to a loudspeaker downstream was implemented. This simple feedback loop was able to successfully suppress thermoacoustic oscillations in a Rijke tube system (this is the system used, as a black box, in this paper). More recent applications of active control to thermoacoustic systems can be found in [16, 17].

1.2 Sensitivity analysis in thermoacoustics

Adjoint-based eigenvalue sensitivity analysis was introduced to thermoacoustic instability by [18]. In a standard sensitivity analysis, the eigenvalues are calculated at one operating point. Then a parameter is changed slightly and the eigenvalues are recalculated at the new operating point. This gives the sensitivity of all eigenvalues to a change in one parameter. In an adjoint sensitivity analysis, the eigenvalues are calculated at one operating point, as before. Then one eigenvalue is selected and the governing equations are reformulated such that the second calculation gives the sensitivity of that eigenvalue to a change in all parameters. In thermoacoustics, usually only a few eigenvalues are of interest, but many parameters can be altered. Adjoint sensitivity analysis is therefore much more efficient than standard sensitivity analysis. Further, the sensitivities calculated with the single adjoint calculation can be combined such that the influence of any passive device can be deduced with one further cheap calculation. Using this technique, [18, 19] were able to determine the shift in growth rate due to the passive drag device and the secondary heater used in the current study. This sensitivity information can be used in optimization algorithms to develop passive control strategies. It should be noted that this is a linear technique, and therefore is only strictly valid for infinitesimal perturbations to parameters. One aim of this paper is to determine the linearity of the parameter sensitivity in a practical system. If the parameter sensitivity is significantly nonlinear, adjoint techniques can still be used, but more intermediate steps are required in the optimization algorithm.

Studies by [1] and [2] provided the first comparison of experimental sensitivity analysis with adjoint-based sensitivity analysis in thermoacoustics. Ref. [1] measured linear growth rates and linear decay rates for a range of different primary heater

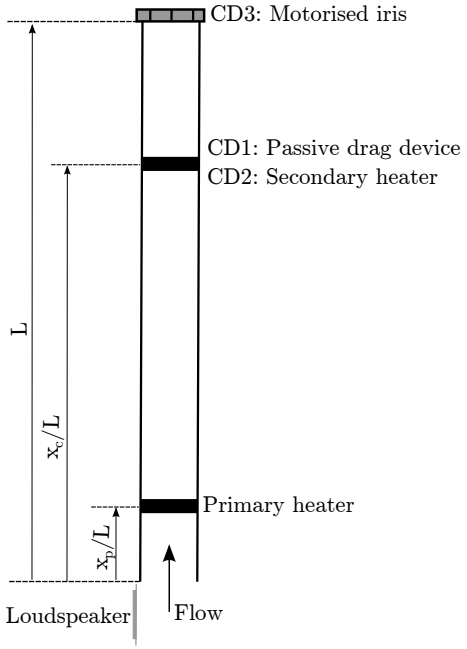

FIGURE 1: Experimental apparatus. CD1 and CD2 are used in section 3. CD3 is used in section 4.

powers and axial locations, x_c/L, of a passive drag device, which in this case was a wire mesh. By subtracting the baseline linear growth rate and linear decay rate, with no passive drag device, from the linear growth and decay rates obtained with a passive drag device installed, they were able to determine the shift in linear growth and decay rate due to the passive drag device. The experimental results were compared with the predictions of adjoint-based sensitivity analysis [19] and agreed well for the shift in growth rate. Ref. [2] measured the linear growth rates and decay rates for a range of different secondary heater powers, P_2, and axial locations, x_c/L. In those studies, (i) the Rijke tube was allowed to reach a steady-state with a primary heater power input of $\approx$ 138 W, (ii) the power input to the primary heater was then abruptly increased to $\approx$ 393 W, and the linear growth rate was measured and (iii) the power input to the primary heater was then abruptly decreased to $\approx$ 138 W, and the linear decay rate was measured. This experimental procedure was repeated for a range of secondary heater powers, P_2, at each axial location (x_c/L = 0.05 to 0.20 and 0.30 to 0.95).

A study by [20] investigated four experimental methods for measuring growth and decay rates on a laminar methane-air burner at a range of stability operating points. The methods included: (i) a harmonic response method in which a loudspeaker harmonically excited the flame in the linearly stable regime at which time the power spectral density (PSD) was measured; (ii) a white noise method in which a stochastic signal was used to excite the flame in either the linearly stable or unstable region, again measuring the PSD of the forced signal; (iii) an impulse response method in which an impulse signal was used to momentarily excite the flame in the linearly stable regime, allowing for a decay rate to be measured as the system returns to a steady-state; and (iv) an active control method which involved switching on and off an active controller in the unstable regime and measuring the growth of thermoacoustic oscillations in time. In method's (i) and (ii) a fitting was applied to the PSD of measured acoustic pressure fluctuations, p', velocity fluctuations, v', and heat release rate fluctuations, $\dot{q}'$, from which the growth rate and frequency was obtained. In method's (iii) and (iv) a fitting was applied to the time-traced signals of p', v', and $\dot{q}'$ from which the growth rate and frequency was obtained. It was found that all four methods were consistent at determining the frequencies, growth and decay rates of thermoacoustic oscillations.

This paper builds on the work of [1], [2] and [20] to develop a more efficient experimental technique to perform experimental sensitivity analysis in thermoacoustics which is compared with the predictions of adjoint-based theory in section 3. The pulsed forcing technique developed in this paper allows the same amount of data to be collected in approximately 1/12 the time of the previous studies, thus allowing for significantly larger data sets to be obtained, which can then be used to refine thermoacoustic models more accurately.

2 EXPERIMENTAL SET-UP AND DATA PROCESSING

2.1 Apparatus

Experiments are conducted on a 1 m long stainless steel Rijke tube with an internal diameter of 47.4 mm and a wall thickness of 1.7 mm (figure 1). For all experiments, the primary heater is at $x_p/L = 0.25$, which is a priori the most destabilizing position [21]. The primary heater is powered by a 640 Watt EA Elektro-Automatik EA-PSI 5080-20 A DC programmable power supply. A G.R.A.S. 46AG 1/2" LEMO microphone with a sensitivity of 12 mV/Pa is used to measure the pressure oscillations. The microphone is angled at 45° towards the inlet of the Rijke tube and placed approximately 55 mm from the bottom of the tube. The raw pressure signal is sampled at 10 kHz, much higher than the anticipated frequencies of the thermoacoustic oscillations, 180 - 190 Hz. Type-K thermocouples are fixed at the centreline of the outlet and inlet, as well as at x/L = 0.05, 0.25, 0.50, 0.75, and 0.95. Temperature data is sampled continuously at 1 Hz and logged with an Omega TC-08 DAQ. A Pro Signal 55-1205 loudspeaker is fixed at the base of the tube, parallel to the flow direction. The loudspeaker is connected to an STA-500 600 W Pro Power amplifier and provided an acoustic signal controlled through National Instruments LabVIEW. All data is acquired through National Instruments BNC-2110 DAQ device using LabVIEW. The ambient air temperature and humidity changed by approximately 8°C and 5%, respectively, over the course of a day.

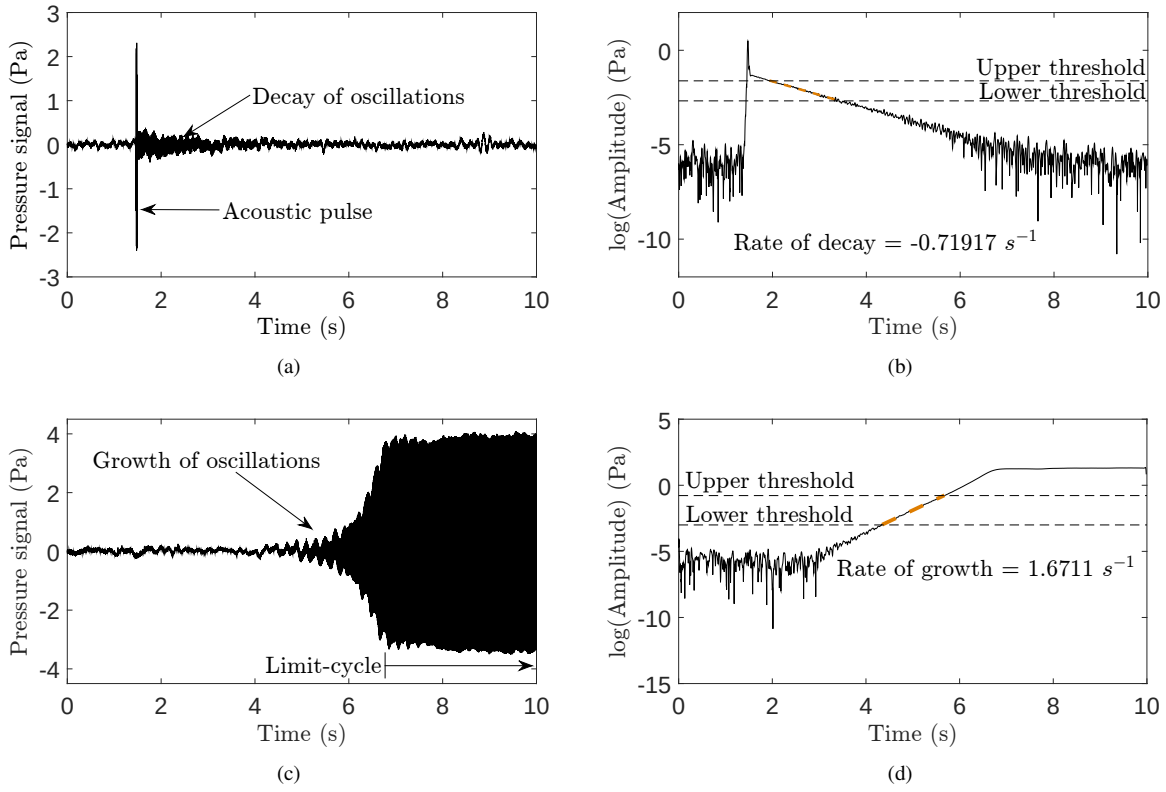

FIGURE 2: (a) Raw pressure signal of a single data point obtained via the pulsed forcing method. (b) Filtered Hilbert transformed signal of the raw pressure signal shown in (a). (c) Raw pressure signal of a single data point obtained as the feedback controller is switched off. (d) Filtered Hilbert transformed signal of the raw pressure signal shown in (c).

For the experiments described in section 3.1, a gauze mesh mounted on two ceramic disks is used as the passive drag device. The experiments described in section 3.2 used an identical second heater with a ISO-TECH IPS 2010 20 V 10 A programmable power supply. The secondary heater is mounted to an automated digital height gauge, allowing it to be traversed through the tube with an accuracy of ± 0.01 mm. A Standa 8MID60-4-H motorised iris is mounted at the outlet of the Rijke tube and used for the experiments described in section 4. This is an array of thin metal segments that slide over each other in order to create an aperture with maximum diameter 60 mm and minimum diameter 4 mm. The iris is controlled via a Standa 8SMC4-USB-B8-1 1-axis stepper motor and could withstand temperatures of approximately 400°C.

2.2 Data acquisition and processing

The linear decay rates are measured in the same way for both control devices. The acquisition of a single data point, for a linear decay rate, is shown in figure 2a and 2b. The acquisition time is 10 seconds, during which time the primary heater had a constant power output of 170 W. After 1.5 s, the loudspeaker forces the flow with a sinusoidal wave of amplitude 2.5 Pa, frequency 175 Hz, and duration 0.05 s. The pressure signal is recorded as these oscillations decay. We apply a bandpass Butterworth filter to the raw signal before taking the Hilbert transform to determine the instantaneous amplitude, $A(t)$, and phase, $\phi(t)$, of the signal, in a similar framework to [22, 23]. The filtered Hilbert transformed signal has a noise-free region of linear decay between two thresholds (figure 2b and 2d). The upper and lower thresholds are set to ensure the linear fit is not influenced by the pulsing signal or noise floor in figure 2b. The linear decay rates are given by $\sigma_r = d(log(A))/dt$.

The linear growth rates are acquired by switching off a feedback controller at $t = 0$, as shown in figure 2c. The controller is an in-house phase-shift amplifier [15]. As the system grows to a stable limit-cycle, the raw pressure signal is measured and then processed via the method described above. The upper and lower thresholds are set to ensure that the linear fit was not influenced by the noise floor or the non-linear effects of the limit-cycle in figure 2d. For all experiments, a simple proportional-integral controller is implemented to ensure that if the resistance of the

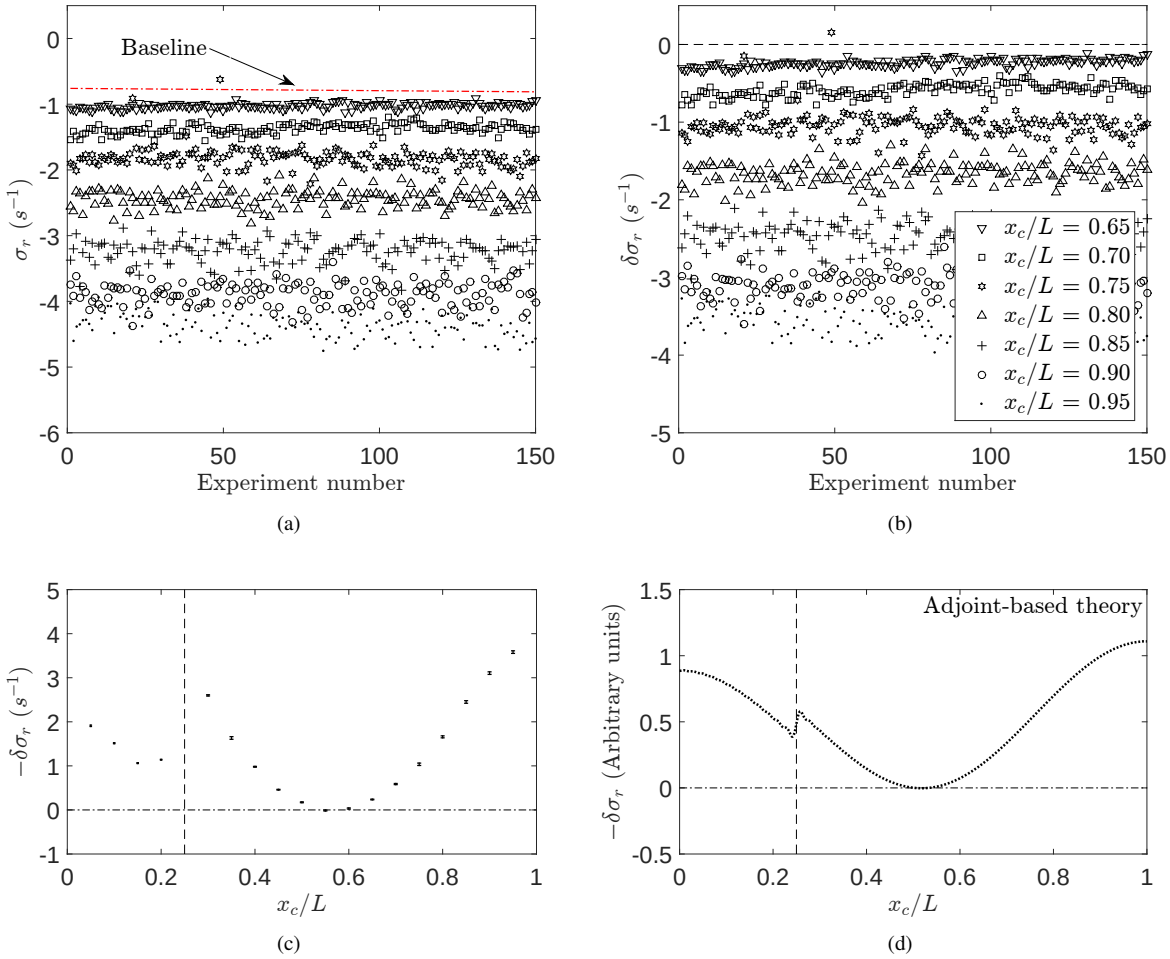

FIGURE 3: (a) Baseline ($\sigma_{r,0}$) and controlled ($\sigma_{r,c}$) linear decay rate for a range of passive drag device positions (x_c/L). (b) Shift in the linear decay rate due to the passive drag device ($\delta\sigma = \sigma_{r,c} - \sigma_{r,0}$). (c) Shift in linear decay rate as a function of x_c/L. (d) Adjoint-based predictions of [18].

heater drifted over the course of the experiments, the power output remains constant, thus not introducing a systematic error into the baseline measurements.

3 SENSITIVITY ANALYSIS VIA PULSED FORCING

This section describes the experimental sensitivity analysis that is performed to ascertain the effect of (i) a passive drag device, and (ii) a secondary heater, on the shift in linear decay rate. Each data point is repeated 150 times so that an uncertainty analysis could be performed. All uncertainty quantification performed in sections 3.1 and 3.2 followed the same procedure outlined in [2]. All error bars are presented for a 95% confidence interval.

3.1 Control via a passive drag device

The experimental method implemented for this control device consisted of the following steps: (i) with no control device installed in the Rijke tube, the system is allowed to reach a steady-state with a primary heater power output of 170 W; (ii) 150 acoustic pulses are given in 10 second intervals resulting in 150 baseline data points for the decay rate; (iii) the passive drag device is introduced at a specific axial location, x_c/L, and then 150 acoustic pulses are given in 10 second intervals resulting in 150 data points for a given x_c/L; (iv) step (iii) is repeated for each axial location, between x_c/L = 0.05 to 0.20 and 0.30 to 0.95; (v) step (ii) is then repeated to determine whether the baseline measurements of the system had drifted over the course of the experiments. The final baseline is determined by averaging both the "before" baseline (step (ii)) and the "after" baseline (step (v))

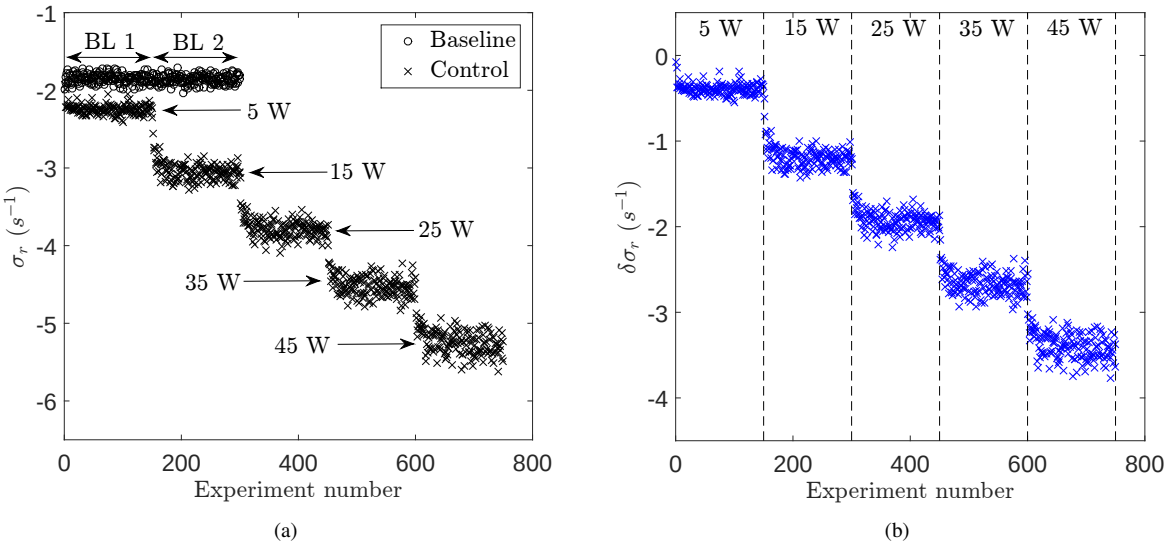

(a) (b)

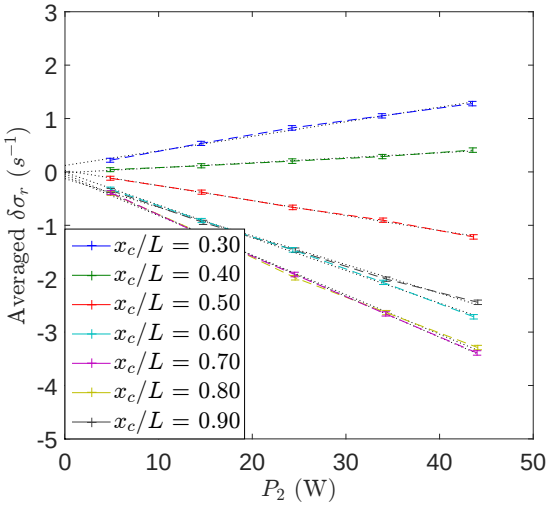

(c)

FIGURE 4: (a) Linear decay rates measured with ($\sigma_{r,c}$) and without ($\sigma_{r,0}$) a secondary heater at $x_c/L = 0.70$. (b) Difference between the linear decay rates measured with and without a secondary heater ($\delta\sigma_{r,c}$), at $x_c/L = 0.70$. (c) Averaged difference between the linear decay rates measured with and without a secondary heater for a range of x_c/L.

and extrapolating linearly in time between the two, thus accounting for any drift in the baseline over the course of the experiment.

The linear decay rates, σ_r, are measured experimentally for a range of x_c/L. The shift in σ_r defined in the theoretical studies of [18] are experimentally determined as

$$\delta\sigma_r(P_1, x_c/L) = \sigma_{r,c}(P_1, x_c/L) - \sigma_{r,0}(P_1) \qquad (1)$$

where P_1 is the primary heater power output, x_c/L is the axial location of the passive drag device, $\sigma_{r,c}$ is the linear decay rate measured with the passive drag device installed, and $\sigma_{r,0}$ is the baseline linear decay rate, measured with only the primary heater installed. To determine the shift in σ_r, the data obtained for each axial location is processed in an identical way. Only the data for x_c/L = 0.65, 0.70, 0.75, 0.80, 0.85, 0.90, and 0.95 is presented (figure 3a and 3b).

Figure 3a shows $\sigma_{r,0}$ and $\sigma_{r,c}$ at a range of x_c/L. It can be seen that as the passive drag device is traversed toward x_c/L =

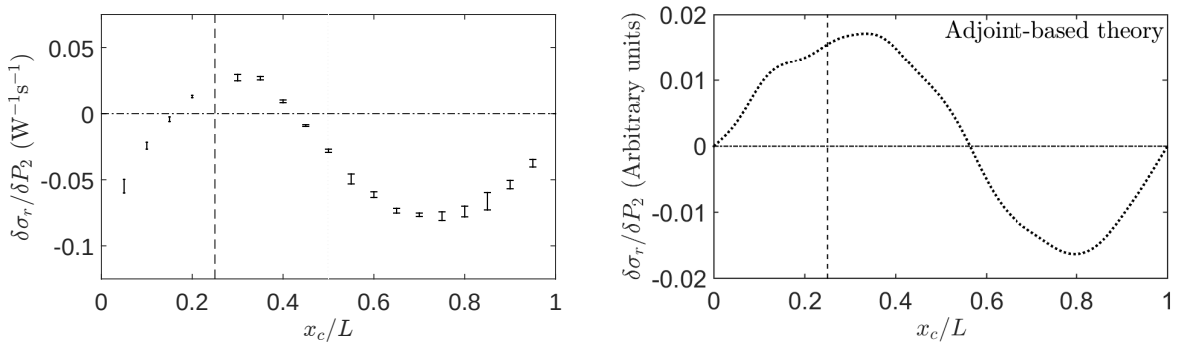

FIGURE 5: (a) Shift in the linear decay rate as a function of x_c/L. (b) Adjoint-based predictions of [18].

0.95, the magnitude of the measured σ_r increases, indicating that the system is becoming more stable and the variance seen in the σ_r measurements increases.

Figure 3b shows the difference between $\sigma_{r,0}$ and $\sigma_{r,c}$ for a range of x_c/L. The shift in linear decay rate due to the introduction of a passive drag device is then calculated by averaging the $\delta\sigma_r$ data obtained and plotting it as a function of x_c/L (figure 3c). It can be seen in figure 3c that the introduction of the passive drag device has a minimal effect when placed at x_c/L = 0.5-0.65 and the largest stabilising effect when placed at x_c/L = 0.95. In comparing figure 3c and 3d it can be seen that the experimental results qualitatively agree well with the adjoint-based predictions of [18].

3.2 Control via a secondary heater

The experimental method implemented for this control case consists of the following steps: (i) with the secondary heater installed at the first x_c/L to be examined, the system is allowed to reach a steady-state with $P_1 = 170$ W and no power to the secondary heater; (ii) at a given x_c/l, 150 acoustic pulses are given in 10 second intervals resulting in 150 baseline data points for the decay rate; (iii) at the same x_c/L used in step (ii), the secondary heater power output, P_2, is increased from 0 to 5 W, at which point 150 acoustic pulses are given in 10 second intervals resulting in 150 data points; (iv) step (iii) is repeated for P_2 = 15, 25, 35, and 45 W, resulting in four sets of 150 data points; (v) step (ii) is repeated twice, with a P_2 output of 0 W, to allow the system time to reach a steady-state. The second set of data is used as the second baseline measurement; (vi) steps (ii) - (v) are then repeated for x_c/L = 0.05 to 0.20 and 0.30 to 0.95.

The σ_r are measured experimentally for a range P_2 and x_c/L. The shift in σ_r defined in the theoretical studies of [18] are experimentally determined as

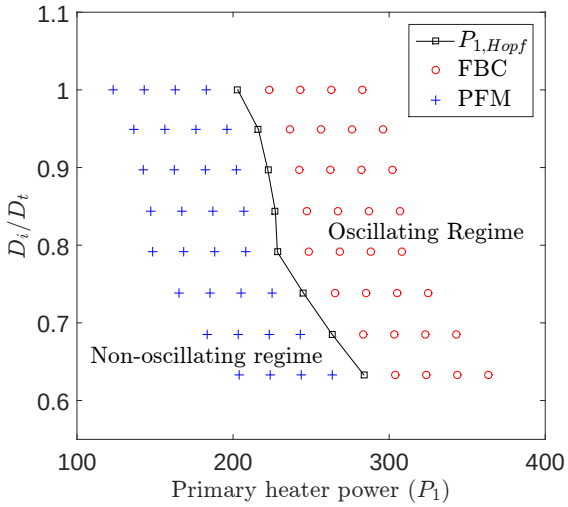

FIGURE 6: Operating region for results presented in section 4. $P_{1,Hopf}$ indicates the stability curve for a variety of iris diameters. FBC denotes points where data is taken via feedback control. PFM denotes points where data is taken via the pulsed forcing method. Spacing between each red circle and each blue cross is 20 W.

$$\delta\sigma_r(P_1,P_2,x_c/L) = \sigma_{r,c}(P_1,P_2,x_c/L) - \ldots \\ \sigma_{r,0}(P_1,x_c/L) \quad (2)$$

where $\sigma_{r,c}$ is the linear decay rate obtained with control, $\sigma_{r,0}$ is the baseline linear decay rate obtained without control, P_1 and P_2 are the same as previously defined. Only the data for x_c/L = 0.70 is presented (figure 4a and 4b).

Figure 4a shows $\sigma_{r,0}$ and $\sigma_{r,c}$, for x_c/L = 0.70. The baseline

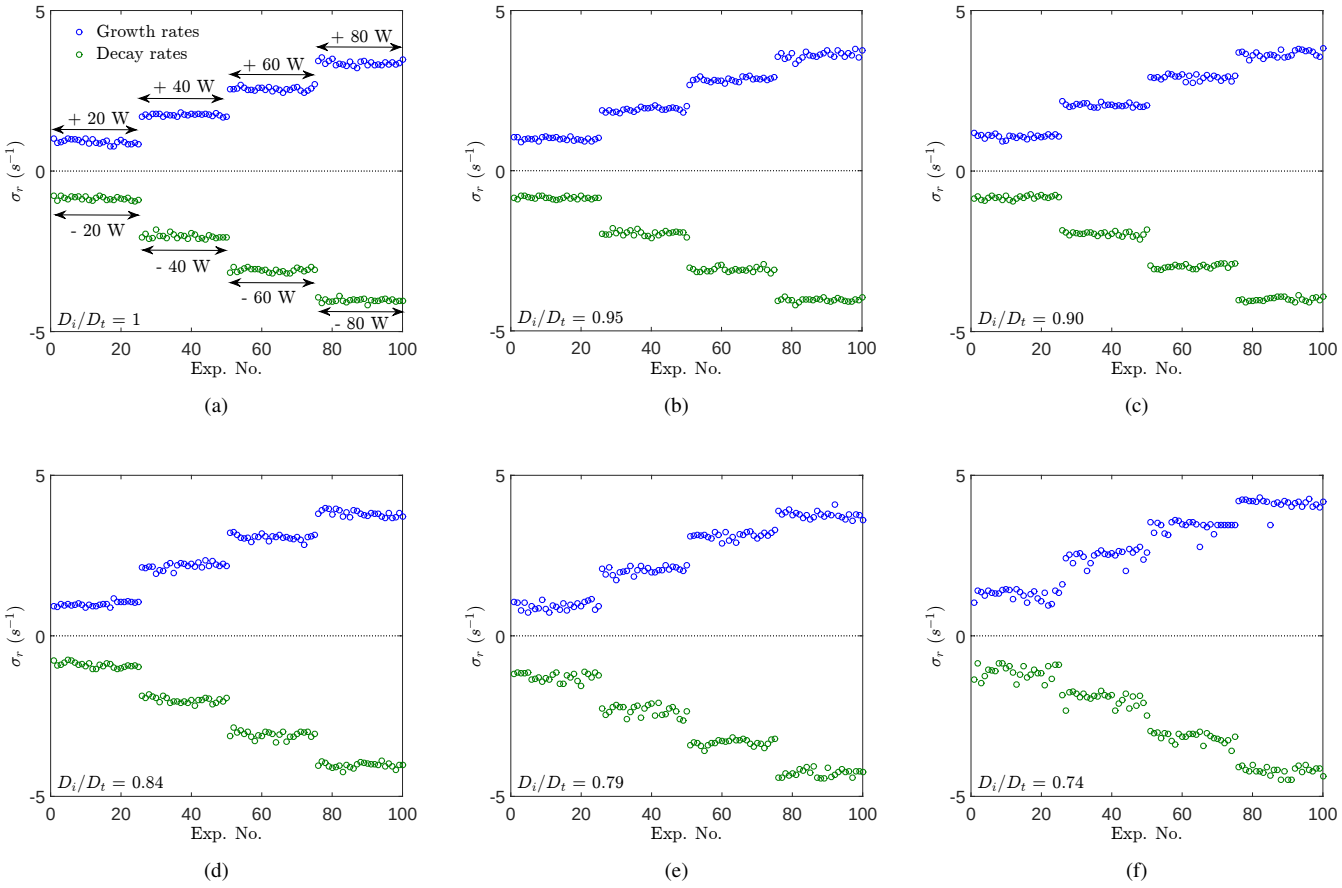

FIGURE 7: Growth rates measured via feedback control and decay rates measured via pulsed forcing for a range of iris diameters.

used in these experiments is determined by averaging both the "before" baseline (B1) and the "after" baseline (B2) and extrapolating linearly in time between the two. This 150 point dataset for the overall baseline is then subtracted from the corresponding dataset of each P_2 tested, resulting in $\delta\sigma_r$ (figure 4b).

It can be seen in figures 4a that as P_2 is increased from 5 W to 45 W, the measured $\sigma_{r,c}$ becomes more negative, showing that the secondary heater has a stabilising effect on the thermoacoustic system is stabilizing.

Similar figures to figure 4b are acquired at $x_c/L = 0.05$ to 0.20 and 0.30 to 0.95. Following this, each set of $\delta\sigma_r$ data is averaged for each P_2. Figure 4c shows $\delta\sigma_r$ for $x_c/L = 0.30$, 0.40, 0.50, 0.60, 0.70, 0.80, and 0.90. These points are chosen so that the changing gradient of $\delta\sigma_r$ with respect to P_2 and x_c/L could be seen. A linear fit is used to extract the gradient of the averaged $\delta\sigma_r$. It can be seen in figure 4c that as the secondary heater is traversed through the tube, the gradient decreases as $x_c/L = 0.30$ to 0.70 and then increases as $x_c/L = 0.80$ to 0.90.

The gradients obtained in figure 4c can then be plotted as a function of x_c/L to show the shift in linear decay rate due to the introduction of a secondary heater, $\delta\sigma_r/\delta P_2$ (figure 5a). Figure 5a shows the results of the experimental sensitivity analysis. Comparing figure 5a and figure 5b it can be seen that the predictions made by [18] have the same form but are shifted vertically. The reason for this is not yet known but indicates a limitation in the model at capturing all of the physical processes occurring in the experiment.

4 EQUIVALENCE OF PULSED FORCING AND FEEDBACK CONTROL FOR PREDICTING ZERO GROWTH RATES

This section compares the pulsed forcing method and the feedback control method by extrapolating their results to find the primary heater power that has zero growth rate. All uncertainty quantification is performed following the same procedure as [2] and the error bars are presented with a 95% confidence interval. It is important that the experimental results obtained in both the oscillatory regime and non-oscillatory regime are compatible

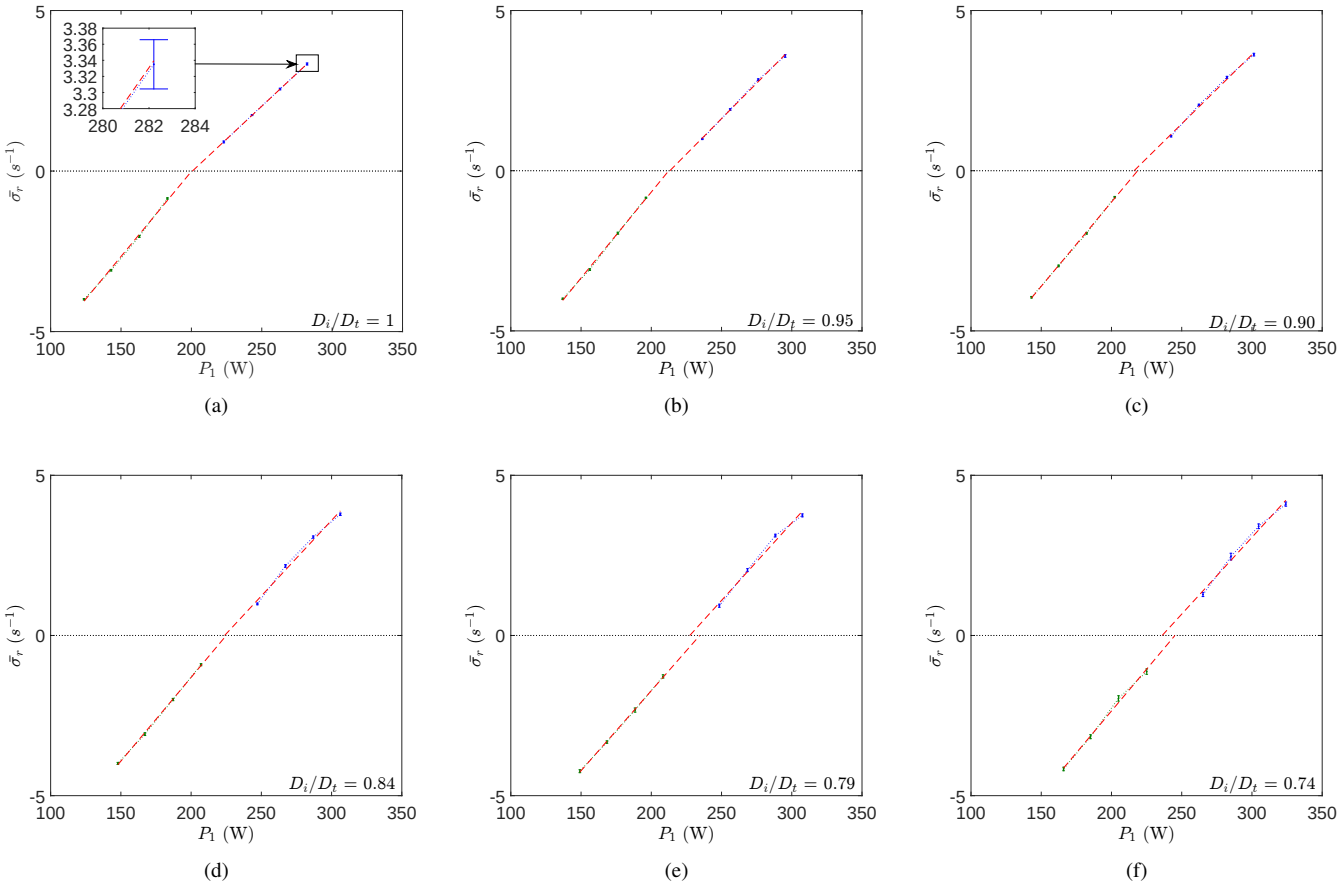

FIGURE 8: Averaged growth and decay rates for a range of D_i/D_t. A first-order polynomial is fitted to each set of growth rate and decay rate data.

with one another and that the pulsed forcing method and/or feedback control method does not introduce bias or systematic error into the results. A simple way to perform this investigation is to measure the Hopf bifurcation point ($P_{1,Hopf}$) for a given iris diameter (D_i/D_t) and then (i) use feedback control to obtain growth rates for $P_1 > P_{1,Hopf}$, and (ii) use the pulsed forcing method to obtain decay rates for $P_1 < P_{1,Hopf}$ (figure 6). With both these sets of data obtained, a straight line is fitted to each set of data to see whether both methods predict the same value of $P_{1,Hopf}$.

The experimental method for this investigation consisted of the following steps: (i) for a given D_i/D_t, obtain the $P_{1,Hopf}$; (ii) at $P_{1,Hopf} + 20$ W the system is allowed to reach a steady-state and then the feedback controller is switched on and then off in 10 second intervals until 25 growth rates are obtained; (iii) step (ii) is repeated in 20 W increments up to $P_{1,Hopf} + 80$ W; (iv) steps (i) - (iii) are repeated for D_i/D_t = 1, 0.95, 0.90, 0.84, 0.79, 0.74, 0.69, and 0.63; (v) at $P_{1,Hopf} - 20$ W the system is allowed to reach a steady-state and then an acoustic pulse is delivered in 10 second intervals until 25 decay rates are obtained; (vi) step (iv) is repeated in 20 W increments up to $P_{1,Hopf} - 80$ W; (vii) steps (v - vi) are repeated for the same range of D_i/D_t.

Figure 6 shows the operating region used for the experiments in section 4. It can be seen that as the iris is closed from D_i/D_t = 1 to 0.63, the primary power input required to transition the system to an oscillatory state increases.

The measured linear growth and linear decay rates for six iris diameters are presented in figures 7a-f. For brevity only D_i/D_t = 1.0, 0.95, 0.90, 0.84, 0.79, and 0.74 are shown here. The mean growth rate and decay rate is then obtained, and presented for each operating point in figure 8.

Straight lines are fitted between the data points, showing that the growth rate data and the decay rate data both extrapolate to nearly the same value of P_1 at $\sigma_r = 0$. This shows that results from the pulsed forcing method are consistent with those from the feedback control method. This is an important result for future work in experimental sensitivity analysis as applied to ther-

moacoustic systems because it shows that either method can be used.

5 Conclusions

The control of thermoacoustic oscillations is an ongoing problem for manufacturers of rocket and gas-turbine engines. Recent work by [18] has demonstrated that adjoint-based sensitivity analysis could be a computationally efficient method to devise good passive control strategies for the suppression of thermoacoustic oscillations.

In this paper, we have extended the work of [1] and [2] to develop a more efficient method of experimental sensitivity analysis and have applied it to a vertical Rijke tube. We introduce an experimental sensitivity analysis method that is suitable for the automated collection of thousands of data points in approximately 1/12 the time of previous work. Our results are compared to results from adjoint-based sensitivity analysis and show good qualitative agreement. In parallel with these results, we have also investigated the equivalence of a pulsed forcing method in the non-oscillating regime and a feedback control method in the oscillating regime. These results show that the pulsed forcing method and the feedback control method are both suitable for experimental sensitivity analysis.

Both methods can be extended to larger rigs. The pulsed forcing method could be achieved by pulsing the fuel supply. The feedback control method is more challenging to implement on larger rigs because of the reliability and operating range of actuators. Nevertheless, this approach has the advantage to industry that the feedback control is not used in operation – it is simply used during the design phase in order to devise optimal passive control strategies.

ACKNOWLEDGMENT

The author would like to acknowledge Mr José Aguilar (University of Cambridge) and Mr Anh Khoa Doan (University of Cambridge) for useful discussions on this work.

REFERENCES

[1] Rigas, G., Jamieson, N. P., Li, L. K. B., and Juniper, M. P., 2016. "Experimental sensitivity analysis and control of thermoacoustic systems". *J. Fluid Mech.,* ***787***(R1), pp. 1–11.

[2] Jamieson, N. P., Rigas, G., and Juniper, M. P., 2016. "Experimental sensitivity analysis via a secondary heat source in an oscillating thermoacoustic system". *Int. J. Spray and Comb. Dyn.,* ***Accepted***, pp. 1–10.

[3] Lieuwen, T. C., and Yang, V., 2005. "Combustion instabilities in gas turbine engines: operational experience, fundamental mechanisms and modeling". *Prog. in Astro. and Aero.*

[4] Lieuwen, T., and Zinn, B. T., 1998. "The role of equivalence ratio oscillations in driving combustion instabilities in low NOx gas turbines". *Symp. (Intl.) on Comb.,* ***27***(2), pp. 1809–1816.

[5] Rijke, P. L., 1859. "On the vibration of the air in a tube open at both ends". *Phil. Mag.,* ***17***, pp. 419–422.

[6] Raun, R. L., Beckstead, M. W., Finlinson, J. C., and Brooks, K. P., 1993. "A Review of Rijke Tubes, Rijke Burners and Related Devices". *Prog. Energ. Combust.,* ***19***, pp. 313–364.

[7] Lighthill, M. J., 1954. "The Response of Laminar Skin Friction and Heat Transfer to Fluctuations in the Stream Velocity". *Proc. of the Royal Society of London. Series A, Mathematical and Physical Sciences,* ***224***(1156), pp. 1–23.

[8] Rayleigh, J. W. S., 1878. "The Explanation of Certain Acoustical Phenomena". *Nature (London),* ***18***, pp. 319–321.

[9] McManus, K. R., Poinsot, T., and Candel, S. M., 1993. "A review of active control of combustion instabilities". *Prog. Energy Combust. Sci.,* ***19***, pp. 1–29.

[10] Candel, S. M., 2002. "Combustion dynamics and control: Progress and challenges". *Proc. Combust. Inst.,* ***29***, pp. 1–28.

[11] Dowling, A. P., and Morgans, A. S., 2005. "Feedback Control of Combustion Oscillations". *Annu. Rev. Fluid Mech.,* ***37***(1), pp. 151–182.

[12] Culick, F. E. C., 1988. Combustion Instabilities in Liquid-Fuelled Propulsion Systems. Tech. Rep. 430.

[13] Katto, Y., and Sajiki, A., 1977. "Onset of oscillation of a gas-column in a tube due to the existence of heat-conduction field: a problem of generating mechanical energy from heat". *Bulletin of JSME,* ***20***(147), pp. 1161–1168.

[14] Sreenivasan, K., Raghu, S., and Chu, B., 1985. "The control of pressure oscillations in combustion and fluid dynamical systems". In 1985 AIAA Shear Flow Control Conf.

[15] Heckl, M. A., 1988. "Active control of the noise from a rijke tube". *J. Sound Vib.,* ***124***(1), July, pp. 117–133.

[16] Zhang, Z., Zhao, D., Han, N., Wang, S., and Li, J., 2015. "Control of combustion instability with a tunable Helmholtz resonator". *Aerosp. Sci. Technol.,* ***41***, pp. 55–62.

[17] Zhao, D., Ji, C., Li, X., and Li, S., 2015. "Mitigation of premixed flame-sustained thermoacoustic oscillations using an electrical heater". *Int. J. Heat Mass Tran.,* ***86***, pp. 309–318.

[18] Magri, L., and Juniper, M. P., 2013. "Sensitivity analysis of a time-delayed thermo-acoustic system via an adjoint-based approach". *J. Fluid Mech.,* ***719***, pp. 183–202.

[19] Magri, L., and Juniper, M. P., 2013. "A Theoretical Approach for Passive Control of Thermoacoustic Oscillations:

Application to Ducted Flames". *J. Eng. Gas Turb. Power,* ***135***(9), pp. 1–9.

[20] Mejia, D., Miguel-Brebion, M., and Selle, L., 2016. "On the experimental determination of growth and damping rates for combustion instabilities". *Comb. and Flame,* ***169***, pp. 287–296.

[21] Saito, T., 1965. "Vibrations of Air-Columns Excited by Heat Supply". *The Japan Society of Mechanical Engineers,* ***8***(32).

[22] Schumm, M., Berger, E., and Monkewitz, P. A., 1994. "Self-excited oscillations in the wake of two-dimensional bluff bodies and their control". *J Fluid Mech.,* ***271***, pp. 17–53.

[23] Provansal, M., Mathis, C., and Boyer, L., 1987. "Bénard-von Kármán instability: transient and forced regimes". *J. Fluid Mech.,* ***182***, pp. 1–22.